Luminescent Platinum(II) Complexes of *N^N⁻^N* Amido Ligands with Benzannulated *N*-Heterocyclic Donor Arms: Quinolines Offer Unexpectedly Deeper Red Phosphorescence than Phenanthridines

Pavan Mandapati,[a] Jason D. Braun,[a] Charles Killeen,[a] Rebecca L. Davis,[a] J. A. Gareth Williams[b*] and David E. Herbert[a*]*

[a] Department of Chemistry and the Manitoba Institute for Materials, University of Manitoba, 144 Dysart Road, Winnipeg, Manitoba, R3T 2N2, Canada
*rebecca.davis@umanitoba.ca, *david.herbert@umanitoba.ca

[b] Department of Chemistry, Durham University, Durham, DH1 3LE, UK
*j.a.g.williams@durham.ac.uk

ABSTRACT

A platform for investigating the impact of π-extension in benzannulated, anionic pincer-type *N*^*N*^*N*-coordinating amido ligands and their Pt(II) complexes is presented. Based on *bis*(8-quinolinyl)amine, symmetric and asymmetric proligands bearing quinoline or π-extended phenanthridine (3,4-benzoquinoline) units are reported, along with their red-emitting, phosphorescent Pt(II) complexes of the form (*N*^*N*^*N*)PtCl. Comparing the photophysical properties of complexes of (quinolinyl)amido ligands with those of π-extended (phenanthridinyl)amido analogs revealed a counter-intuitive impact of site-selective benzannulation. Contrary to conventional assumptions regarding π-extension, and in contrast to isoenergetic lowest energy absorption bands and a red shift in fluorescence from the organic proligands, a blue shift of nearly 40 nm in the emission wavelength is observed for Pt(II) complexes with more extended *bis*(phenanthridinyl) ligand π-systems. Comparing the ground state and triplet excited state structures optimized from DFT and TD-DFT calculations, we trace this effect to a greater rigidity of the benzannulated complexes, resulting in a higher energy emissive triplet state, rather than to a significant perturbation of orbital energies caused by π-extension.

INTRODUCTION

The utility of phosphorescent platinum(II) complexes in chemosensing,[1-2] bioimaging,[3-5] and light-emitting diodes[6-9] is owed both to the large spin-orbit coupling (SOC) constant of the third row transition metal, which promotes the formally forbidden $T_1 \rightarrow S_0$ radiative process, and to a well-developed coordination chemistry where ligand design is used to control color and enhance emission.[10-11] Amongst the most brightly luminescent Pt(II) complexes, cyclometallating ligands predominate, particularly those based on 2-phenylpyridine (ppy).[12-14] Tridentate derivatives[15-19] that combine *N*-heterocycles and *C*-metallated aryl rings have also been reported (Figure 1a). In such ligand sets, the synergistic combination of strong σ-donation (C–Pt bond) and the π-accepting nature of the heterocycle stabilizes charge-transfer (CT) excited states over metal-centered (MC) ones, limiting undesirable non-radiative decay and ligand photolability through population of d orbitals with metal-ligand anti-bonding character.[20] The multidentate, chelating ligand arrangement also increases the rigidity of the complex, suppressing excited-state distortions that can contribute to non-radiative decay pathways. This may have an additional effect of enhancing color purity by reducing contributions from longer-wavelength Franck-Condon vibrational components, often particularly desirable in the design of OLED emitters.[21-22] These frameworks also increase the stability of a complex, important in high temperature processing common to device fabrication by evaporation.[23]

Once a promising ligand framework has been identified, tuning the photophysical properties commonly involves either substitution of a ligand with donor/acceptor groups or expansion of a ligand's conjugated π-system. Both strategies are understood to impact absorption/emission spectra by influencing the relative energies of the frontier orbitals (HOMO/LUMO), though not always in an obvious manner. For example, despite the prevailing expectation that extending π-conjugation via benzannulation of aromatic molecules or ligands will induce bathochromic (red) shifts in absorption/emission spectra by stabilizing ligand-based π* acceptor orbitals, both red and blue shifts in absorption/emission bands have been recorded for Pt(II) complexes of benzannulated derivatives of 1,3-*bis*(2-pyridylimino)isoindoline (BPI) ligands (Figure 1b).[24-26] Using a

series of benzannulated (BPI)PtCl complexes, Thompson and colleagues[27] detailed a general theoretical framework for understanding and predicting the direction of energy shifts caused by benzannulation. In that paradigm, the site of benzannulation is critical and the shift in absorption/emission energy can be traced to a selective stabilization or destabilization of the HOMO or the LUMO.

With this background in mind, the *bis*(quinolinyl)amido (BQA) ligand attracted our attention as an alternative *N*^*N*^*N*-binding ligand, potentially well-suited to the construction of Pt(II)-based emitters (Figure 1c).[28-31] First, this tridentate, pincer-like amido ligand bears two all-sp^2 quinolinyl heterocyclic donor arms and forms robust, square planar coordination compounds with Group 10 elements with 5-membered chelate rings (in contrast to the 6-membered rings of Pt(BPI)Cl).[28] Second, unlike *N*^*C*^*N* cycloplatinated complexes, which often require forcing conditions to prepare and which incorporate a central carbon donor whose strong *trans* influence can labilize *trans* disposed ligands,[32] ligands that feature anionic amido donors can be installed following more accessible deprotonation of an N–H group. Third, the strong, rigid, planar binding of the tridentate ligand suggests that a triplet state populated by light absorption might exhibit only small structural distortions in the excited state, potentially favoring emission over non-radiative decay processes. Finally, thinking of *bis*(quinolinyl)amine as a framework, the quinolinyl arms provide a conceptual site for benzannulation to 3,4-benzoquinoline (phenanthridine) where the site-selection for π-extension should not impact the coordinating ability of the tridentate ligand; such modification contrasts with 2,3-benzannulation, for example, that converts quinoline to acridine. We accordingly report here on the synthesis and luminescence properties of Pt(II) complexes of BQA pincer-type amido ligands and their benzannulated analogs. We find that for this ligand design, neither of the prevailing predictive paradigms for understanding the impact of benzannulation on photophysical properties is appropriate: absorption and emission are not impacted in the same direction by benzannulation.

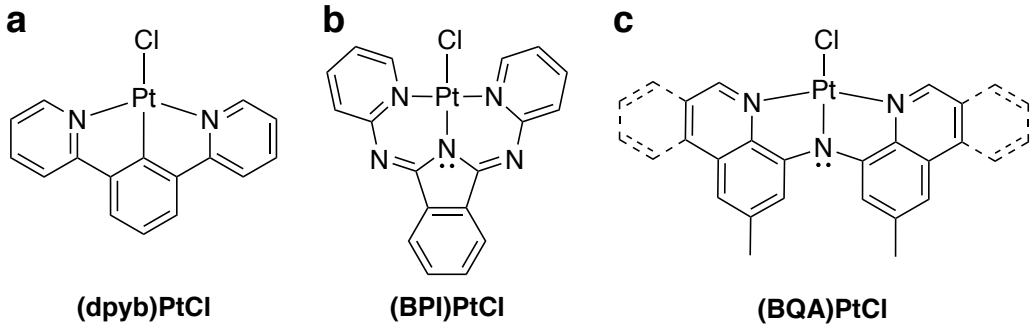

Figure 1. Structures of (a) (dpyb)PtCl featuring an *N^C^N*-coordinating, tridentate cyclometallated ligand, dpybH = 1,3-di(2-pyridyl)benzene; (b) (BPI)PtCl containing an *N^N⁻N*-coordinating tridentate ligand, BPI = 1,3-*bis*(2-pyridylimino)isoindoline; (c) (BQA)PtCl-derived complexes containing benzannulated, tridentate *N^N⁻N*-coordinating ligands with either quinolinyl or phenanthridinyl donor arms, BQA = *bis*(8-quinolinyl)amine.

RESULTS AND DISCUSSION

Ligand Preparation and Scope

Taking *bis*(8-quinolinyl)amine as our conceptual starting point, we targeted methyl-substituted *bis*(8-(6-methyl)quinolinyl)amine (**L1**) and *bis*(4-(2-methyl)phenanthridinyl)amine (**L3**) proligands, together with a "mixed" analog that incorporates one quinoline and one phenanthridine (**L2**). These compounds were prepared via Pd-catalyzed Buchwald-Hartwig coupling of methyl-substituted amino/bromoquinolines and phenanthridines (Scheme 1). 6-(Methyl)quinolines amenable for cross-coupling were accessible via the Skraup reaction,[33] while 2-methylphenanthridine derivatives were assembled using one-pot Suzuki coupling/condensation reactions.[34] In both cases, methyl substitution improves precursor yields over unsubstituted derivatives. Proligand synthesis proceeded efficiently and the *bis*(*N*-heterocyclic)amines **L1** and **L2** were isolated in high yields (80-90%) as yellow solids following chromatography. **L3** has been previously described.[35]

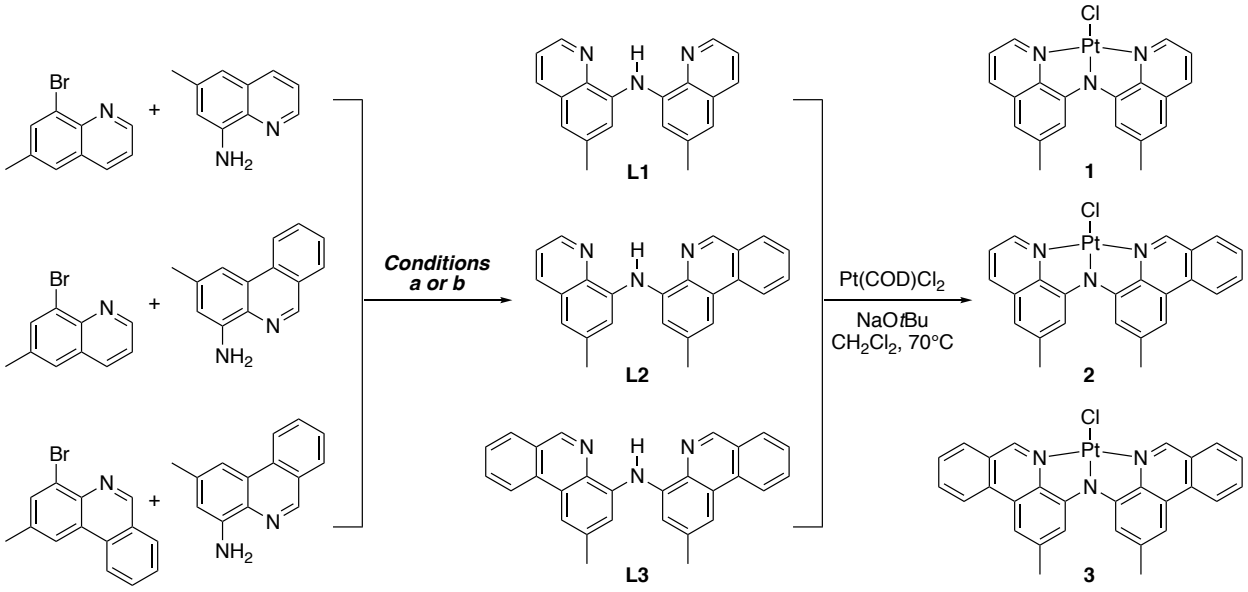

Scheme 1. Synthetic routes to proligands **L1**, **L2** (conditions *a*) and **L3** (conditions *b*)[35] and their corresponding Pt(II) complexes **1**, **2** and **3**. Conditions: *a*: $Pd_2(dba)_3$, *rac*-BINAP, NaO*t*Bu, toluene, 150 °C; *b*: $Pd(OAc)_2$, dppf, NaO(*tert*-pentoxide); toluene, 150 °C.

The *N*^*N*^*N*-coordinated Pt(II) complexes (**1**/**2**/**3** from **L1**/**L2**/**L3**, respectively) were prepared upon reaction of the appropriate proligands with $Pt(COD)Cl_2$ in refluxing dichloromethane, in the presence of a sodium alkoxide base. The complexes precipitated over the course of the reaction as deep red solids. Their solubility is generally poor in standard organic solvents and benzannulation was found to further decrease the solubility. Nevertheless, ^{1}H NMR spectroscopy in solution could be used to verify ligand coordination, which was followed by the shift of the diagnostic [C*H*] resonance in the 6-position of the phenanthridinyl arms of **L2** and **L3** (Table S1). Compound structures could thereby be confirmed by NMR spectroscopy, and their purity was established by elemental analysis.

The crystal structure of **1** is shown in Figure 2 (the structure of **3** was previously reported[35]). In the solid state, the ligands are rigidly planar and bind meridionally to the metal centre. The three nitrogen donor atoms of the ligands are coplanar with the

coordinated metal atom, resulting in an essentially flat molecular structure. The structure of **1** does not include any solvent in the crystal lattice, while crystals of complex **3** suitable for X-ray diffraction could only be obtained with a co-crystallized molecule of chloroform[35] (Figure S1). In the structure of **1**, close intermolecular π-π interactions are observed (~3.3 Å), while only hydrogen bonding with co-crystallized $CHCl_3$ can be seen in the structure of **3**. The decreasing solubility in the order **1** > **2** > **3** is presumably attributable to similar π-π interactions as seen in the structure of **1**, likely enhanced by benzannulation. Crystals with sufficient long-range order for good diffraction could only be obtained if these intermolecular interactions could be disrupted, for example, through inclusion of a hydrogen bond donor solvent in the crystal lattice. As solids, all three platinum complexes show high thermal stability, which varies a little with the degree of benzannulation: 5% weight reduction was observed at temperatures of 386 °C (**1**), 430 °C (**2**) and 378 °C (**3**), respectively (Figure S2).

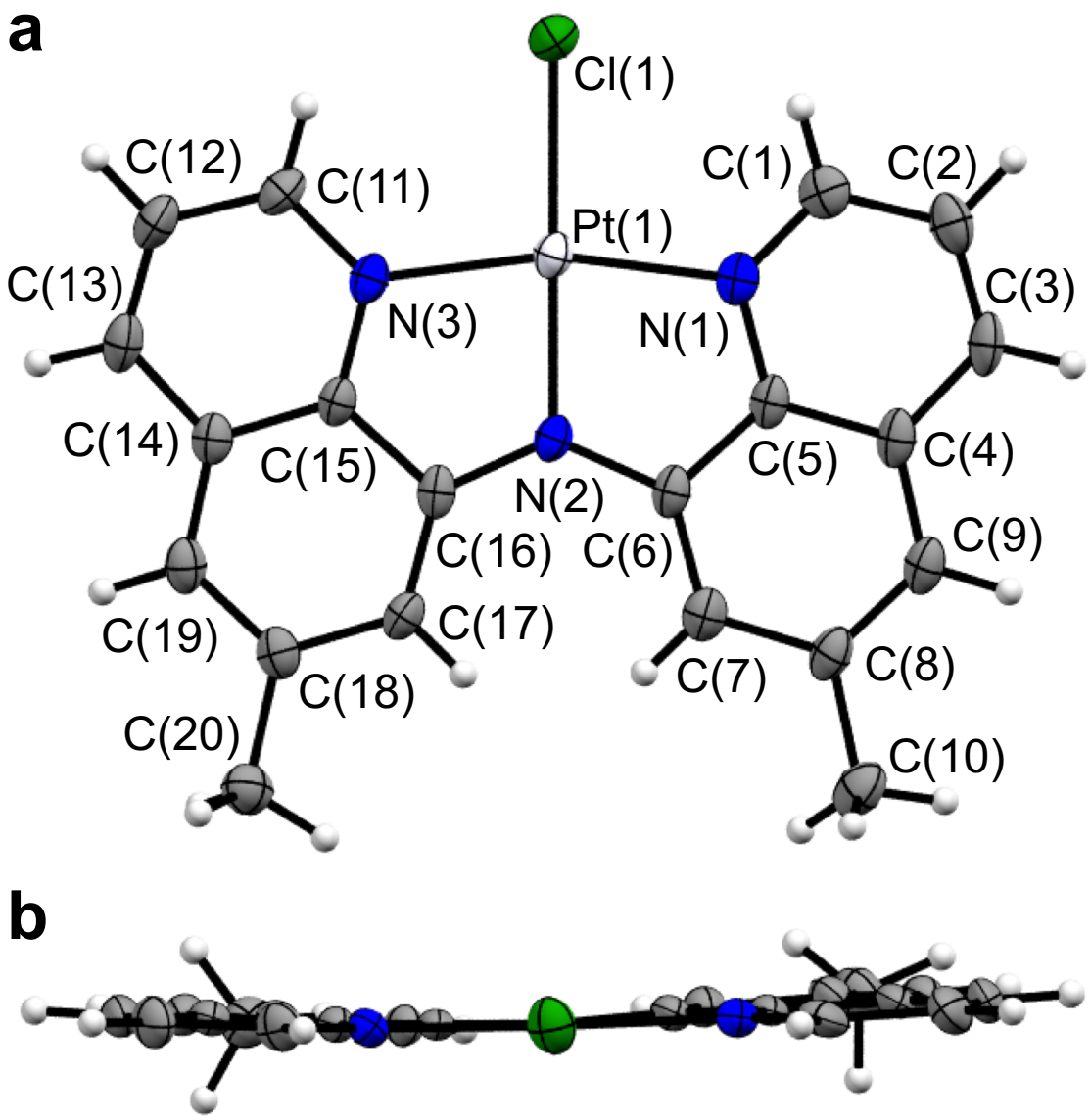

Figure 2. Solid-state structure of **1** shown (a) perpendicular to the metal square plane, and (b) along the Cl–Pt–N(2) axis. Thermal ellipsoids are shown at 50% probability and hydrogen atom labels are omitted for clarity. Selected bond distances (Å) and angles (°): Cl(1)–Pt(1) 2.339(1), N(1)–Pt(1) 1.998(4), N(2)–Pt(1) 1.971(4), N(3)–Pt(1) 2.000(4), N(1)–C(1) 1.329(6); N(1)-Pt(1)-N(3) 165.23(17), N(2)-Pt(1)-Cl(1) 179.42(11), N(1)-Pt(1)-Cl(1) 97.55(12), N(3)-Pt(1)-Cl(1) 97.10(12), N(2)-Pt(1)-N(1) 82.56(16), N(2)-Pt(1)-N(3) 82.77(16), C(6)-N(2)-C(16) 130.7(4).

Photophysical Properties

Absorption and emission spectra for the three proligands in dichloromethane solution at room temperature are shown in Figure 3 and associated data are compiled in Table 1. In its absorption spectrum, the *bis*(quinolinyl)amine proligand **L1** displays two main bands, one deep in the UV region at 270 nm and a longer wavelength band extending into the visible region, centered at 403 nm. The *bis*(phenanthridinyl) analogue **L3** has a similar, but broader, long-wavelength band with a blue-shifted λ_{max} (388 nm), an intense band at 253 nm, and a band at 299 nm that has no counterpart in the spectrum of **L1**. The "mixed" quinoline-phenanthridine system **L2** shows features corresponding to both **L1** and **L3**; in fact, its spectrum is nearly identical to that simulated from an average of **L1** and **L3** (Figure S3). While the peak maximum of the long wavelength band appears blue shifted in the phenanthridine-containing systems **L2** and **L3** relative to that of the *bis*(quinolinyl)amine **L1**, it should be noted that this band tails further into the visible for **L2** and **L3**, with higher absorption at $\lambda > 415$ nm, suggesting that the lowest energy transitions may indeed be lower in energy in the phenanthridine proligands with their more extended π systems. For comparison, the first-excited singlet state energies (E_S) of quinoline and phenanthridine are 31850 and 28590 cm^{-1} respectively.[36]

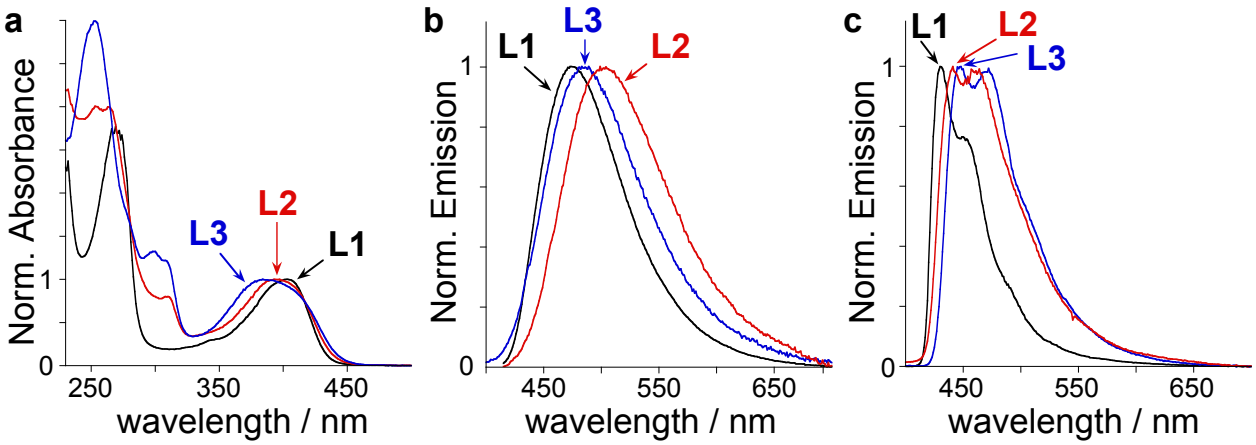

Figure 3. (a) UV-visible absorption spectra of proligands **L1-L3** in CH_2Cl_2 solution at 295±1 K; Photoluminescence spectra in (b) CH_2Cl_2 solution at 295±1 K and (c) EPA at 77 K.

Table 1. Absorption and emission data of proligands[a] and Pt(II) complexes[b]

	Absorption λ_{max}/nm (ε / mM^{-1} cm^{-1})	Emission λ_{max}/nm[c]	Φ_{lum} (%)[c,d]	τ / ns[e]	k_r /10^3 s^{-1}[f]	Σk_{nr} /10^5 s^{-1}[g]	k_Q^{O2} /10^9 M^{-1} s^{-1} [h]	Emission 77K[i]	
								λ_{max}/nm	τ / ns
L1	269 (28.4), 344 (3.2), **403** (9.8)	474	0.55	--[j]	--	--	--	431, 451	3.5
L2	254 (26.0), 264 (27.1), 310 (7.4), **395** (9.0)	503	0.25	--[j]	--	--	--	441, 461	3.8
L3	253 (65.2), 299 (22.0), 308 (sh), **388** (15.9)	485	0.20	--[j]	--	--	--	447, 471	3.2
1	301 (35.3), 340 (6.0), 356 (4.9), 381 (1.6), **501** (9.2)	738	0.081	1800 [230]	0.49	5.6	1.7	696, 763	2200
2	284 (23.7), 315 (21.8), 338 (15.3), 354 (9.8), 405 (3.0), **502** (8.5)	740	0.13	1000 [180]	1.3	10	2.1	692, 756	3000
3	265 (28.0), 321 (16.1), 338 (13.6), 355 (9.6), 405 (2.6), **503** (4.9)	703	0.18	2500 [190]	0.72	4.0	2.2	663, 727	18300

[a] In CH_2Cl_2 at 295±1 K and in EPA (diethyl ether/isopentane/ethanol, 2:2:1 v/v) glass at 77 K; λ_{ex} = 400 nm. [b] In degassed CH_2Cl_2 at 295±1 K, except where indicated otherwise. [c] Emission maxima and photoluminescence quantum yields Φ_{lum} determined from spectra recorded using a Synapse CCD detector. [d] Measured in deoxygenated solution (**1-3**), using $[Ru(bpy)_3]Cl_{2(aq)}$ as the standard. [e] Luminescence lifetimes in deoxygenated solution (**1-3**). Values in air-equilibrated solution are given in square parenthesis. [f] Radiative (k_r) and non-radiative (Σk_{nr}) rate constants estimated from quantum yield and lifetime, assuming unitary population of the emissive state upon light absorption: $k_r \sim \Phi / \tau$; $k_{nr} \sim (1-\Phi) / \tau$. [g] Bimolecular Stern-Volmer constant for quenching by molecular oxygen, estimated from the lifetimes in deoxygenated and air-equilibrated solution, and assuming $[O_2]$ = 2.2 mmol dm^{-3} at atmospheric pressure of air. [h] In diethyl ether / isopentane / ethanol (2:2:1 v/v). [i] Emission spectra at 77 K were recorded using a Hamamatsu R928 PMT detector. [j] The lifetimes of the proligands are probably < 1 ns but the intensity is too weak to allow reliable deconvolution from the instrument response and a precise value to be obtained.

Time-dependent density functional theory (TD-DFT) analysis assigns the lowest energy transition for all three proligands as HOMO→LUMO in nature (see Tables S2-S4 and Figures S4-S6). Population analysis shows the HOMOs are comprised largely of the amino (N-H) lone pair, with contributions from the hydrocarbon portions of the heterocycle arms (see Figures S7-S8 and Tables S5-S7). Interestingly, for both **L2** and

L3, the HOMO does not significantly include any orbital density located on the most distal fragments of the benzannulated ligand moieties, *i.e.*, at the site of benzannulation. In contrast, the LUMOs of all three proligands are comprised of out-of-phase (π*) contributions from the *N*-heterocycle π systems; the LUMO of **L2** (and **L3**) are heavily influenced by benzannulation. The distinctive bands at 299 nm in the spectra of phenanthridinyl-containing **L2** and **L3**, but absent from the spectra of **L1**, arise primarily from HOMO–1→LUMO transitions. The HOMO–1 orbitals of **L2** and **L3** are higher in energy than in **L1**, and this transition is therefore likely buried deeper in the UV for the smallest ligand **L1**. The contribution from the phenanthridinyl moiety is clear here - the HOMO–1 of the asymmetric **L2** is mostly located on the phenanthridine moiety, with very little contribution from the quinolinyl arm.

The proligands are weakly fluorescent in solution at room temperature, each displaying a broad unstructured emission band with λ_{max} in the range 474 – 518 nm, quantum yields < 1% and lifetimes < 1 ns at room temperature (Figure 3b, Table 1). Considering the impact of benzannulation, the *bis*(quinolinyl)amine proligand **L1** emits at higher energy than the phenanthridine analogues **L2** and **L3**, in line with the aforementioned differences in E_S for quinoline and phenanthridine. Comparing the room temperature and low temperature spectra, the red shift of the mixed quinoline–phenanthridine proligand **L2** relative to **L3** at ambient temperature might be explained in terms of more pronounced charge-transfer character between the different aromatic arms (quinoline→phenanthridine), evident in transitions involving the frontier orbitals in the asymmetric **L2**, which is destabilized at 77 K (Figure 3c).

Photophysical data for the corresponding platinum complexes are also compiled in Table 1. The most striking difference in the spectra of the metal complexes compared to the corresponding proligands is the appearance of an intense, broad band centered close to 500 nm. This band evidently accounts for the strong, deep red color of the complexes. The substantial displacement of the band to lower energy by some 5000 cm^{-1} relative to the lowest energy band in the proligands is intuitively consistent with the deprotonation of the amine N–H that accompanies complexation. This would be expected to increase the energy of highest occupied orbitals, while the vacant heterocycle-based π* orbitals may be conversely lowered in energy upon binding to Pt(II). The resulting

decrease in the frontier orbital energy gap would produce the observed red shift, very much in line with those observed for BPI ligands (Figure 1) upon binding to transition metal ions.[25, 27]

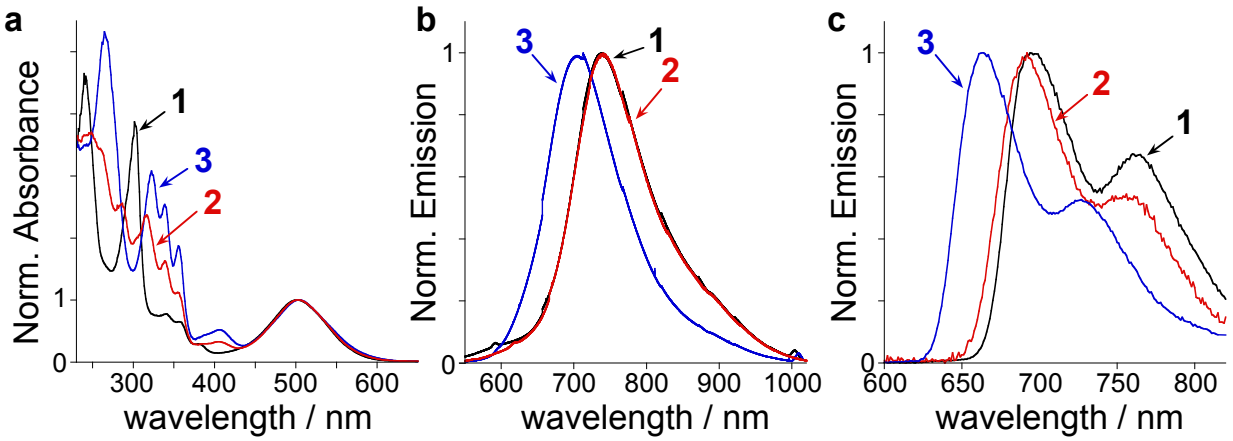

Figure 4. (a) UV-visible absorption spectra of Pt(II) complexes **1-3** in CH_2Cl_2 solution at 295±1 K; Photoluminescence spectra in (b) CH_2Cl_2 solution at 295±1 K and (c) EPA at 77 K.

As with the proligands, the main difference between the *bis*(quinolinyl) complex **1** and *bis*(phenanthridinyl) complex **3** is the stronger absorption of the latter in the 300–350 nm region. The "mixed" quinoline-phenanthridine system **2** again has an absorption spectrum that closely matches that simulated from the average of **1** and **3** (Figure S9). All of the complexes are luminescent in deoxygenated solution at room temperature, emitting in the deep red / near-infrared region of the spectrum (Figure 4b, Table 1). The emission tails into the 800–1000 nm region, a part of the spectrum where the sensitivity of conventional photomultiplier tubes falls off steeply. The recording of the emission spectra was better achieved using a CCD detector (see Experimental Section for details).

The spectra each show a single, unstructured band that is relatively narrow compared to many red/NIR-emitting transition metal-based phosphors (FWHM ~ 2300 cm^{-1}).[37-40] Interestingly, and counterintuitively, amongst the series **1-3**, the *bis*(phenanthridinyl) complex **3** unequivocally emits at higher energy than the quinoline-containing complexes, despite the more extended conjugation of phenanthridine compared to quinoline and the isoenergetic absorption maxima. Furthermore, the

spectrum of the mixed quinoline-phenanthridine **2** is essentially identical to that of *bis*(quinoline) **1**, suggesting that the emissive excited state in the former involves the quinoline rather than the phenanthridine. At 77 K, a vibrational 0,1 band is resolved to low energy of the main 0,0 component in each case,[41] but the trend in emission energies **3** > **2** ~ **1** is retained (Figure 4c). This counterintuitive trend is reminiscent of an unexpected blue-shift, observed by Thompson and co-workers, in the phosphorescence of Pt(*N^C*-dbq)(dpm) compared to Pt(*N^C*-bzq)(dpm), where dbq and bzq are cyclometallated dibenzo[*f,h*]quinoline and benzo[*h*]quinoline respectively (dpm = *O^O*-coordinated dipivolylmethanoate),[42] and in benzannulated Pt(BPI)Cl complexes.[27] In those cases, however, the impact of benzannulation on absorption matched that on emission. We also observed a similar effect in the luminescence of dinuclear Cu(I) complexes $[(P\text{^}N)\text{Cu}]_2(\mu\text{-X})_2$ with *P^N*-coordinating phosphine-pyridine ligands based on quinolines and phenanthridines (X = halide): the luminescence of the more conjugated phenanthridine-based complexes was blue-shifted relative to the quinoline analogues.[43] Here, the absorption maxima are unchanged by benzannulation, while emission is starkly affected. We return to the likely origin of this effect in the next section. The luminescence lifetimes in deoxygenated solution are of the order of a microsecond (Table 1), which is quite typical of cyclometallated Pt(II) complexes and indicative of phosphorescence from a formally forbidden triplet state that is facilitated by the spin-orbit coupling associated with the metal. The lifetimes are an order of magnitude shorter in air-equilibrated solutions, indicating quenching of the triplet excited state by molecular oxygen: the bimolecular rate constants for quenching are around 2×10^9 M^{-1} s^{-1}.

The luminescence quantum yields are in the range of 0.1–0.2 %. A close match of the excitation spectra with the absorption spectra suggests that the emitting triplet state forms with high efficiency, irrespective of the state to which light absorption occurs (as typically observed in most phosphorescent Pt(II) complexes thanks to efficient intersystem crossing to the triplet state). Quantum yields are then determined by the relative values of the radiative k_r and non-radiative $\sum k_{nr}$ rate constants. Assuming that the emitting state is indeed formed with unitary efficiency, they can be estimated as follows: $k_r = \Phi / \tau$ and $\sum k_{nr} = (\tau^{-1} - k_r)$. The values thus obtained are compiled in Table 1. From these data, it can be seen that the low quantum yields are a combined result of low k_r

values in the range 500–1300 s^{-1} and high $\sum k_{nr}$ up to 10^6 s^{-1}. In contrast, the most efficient red-emitting Pt(II) complexes reported to date (albeit emitting at shorter λ_{max} ~650 nm) have k_r values almost two orders of magnitude higher and $\sum k_{nr}$ up to two orders of magnitude lower.[44] The low k_r values may reflect a relatively low degree of metal character in the triplet state, given the highly conjugated nature of the organic ligand. Indeed, the systems bear some resemblance to the units found in Pt(II) phthalocyanines and Pt(II) porphyins, where quantum yields are limited by low k_r.[41] TD-DFT calculations support this interpretation in terms of limited metal character, as discussed in the next section. They also reveal substantial distortion of the excited triplet state relative to the ground state, which could account for the large $\sum k_{nr}$ values.

Amongst the three complexes, the highest $\sum k_{nr}$ value is found for that which emits at lowest energy and vice versa, qualitatively in line with intramolecular vibrational deactivation of electronic excited states and the "energy gap law".[45] There is no clear-cut trend in k_r. A smaller k_r for the highest-energy emitter **3** evidently limits the quantum yield, which is not significantly higher than for **2**, despite having the lowest $\sum k_{nr}$ value.

DFT Calculations

Density functional theory (DFT) and time-dependent DFT (TD-DFT) calculations were carried out on the three complexes (**1**/**2**/**3**) to interpret the trends observed in the photophysical properties. Inspecting the orbital densities of the frontier orbitals and the LUMO+1 illustrates the similarities between the sets of complexes (Figure 5 and Figure S10). For example, the HOMOs of all three Pt(II) complexes are comprised of nearly even contributions from the metal center, the amido 2p lone pair, and the C_6 ring of the *N*-heterocyclic ligand arms (for Hirshfeld populations, see Tables S8-S10 and Figure S11). In comparison, the unoccupied orbitals are almost completely localized on the C_5N rings of the *N*-heterocycles, split equally in the symmetric complexes (**1**/**3**) with the LUMO weighted more heavily (64%) on the phenanthridinyl arm in the asymmetric complex (**2**).

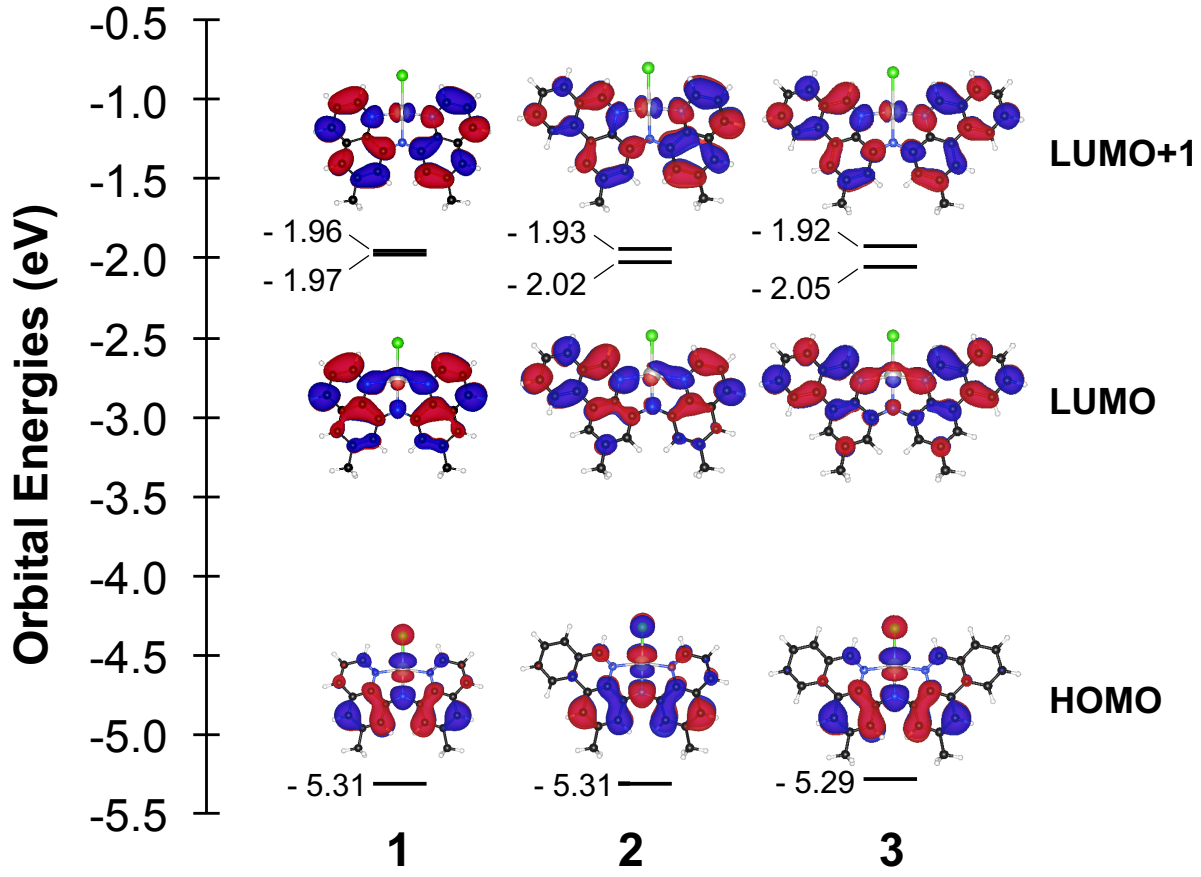

Figure 5. Orbital diagrams of the HOMO, LUMO and LUMO+1 of **1**, **2** and **3** shown with isovalues of 0.02.

The major difference between the absorption spectra of the three metal complexes is the appearance of additional prominent peaks at higher energy (300-430 nm) that grow in intensity when comparing complexes of **2** and **3**, and therefore can be attributed to the phenanthridinyl arms. TD-DFT (see Tables S11-S13, Figures S12-S14) assigns these to HOMO→LUMO+2 transitions (**2**) and HOMO→LUMO+2/HOMO→LUMO+3 transitions (**3**). These virtual orbitals are largely π-anti-bonding combinations on the π-extended portion of the phenanthridinyl ligand arms. The corresponding orbitals (LUMO+2) are at much higher energy for the smaller quinolinyl π-system of **1**, pushing these transitions further into the UV.

For the lowest energy absorption manifold, (d_{Pt}+p_N)-to-π* metal-to-ligand charge transfer character is evident from the population analyses and MO diagrams. TD-DFT calculations show that the peak with the highest oscillator strength in all three complexes is composed of a HOMO→LUMO+1 transition; the HOMO→LUMO excitation does not contribute significantly to this band. Fragment contributions calculated using the Hirshfeld atomic population method[46] reveal that for all three complexes, the HOMO/LUMO+1 pair are more coextensive than the HOMO/LUMO pair, thanks to sizeable contributions from the C_6 rings of the heterocyclic arms. While the LUMO+1 experiences a slight destabilization with π-extension, this is offset by a small perturbation in the HOMO energy of **3** (Table 2). Thus, while the LUMO is actually stabilized progressively with benzannulation (**3** > **2** > **1**), there is little change to the wavelengths of the lowest energy absorption manifold. Indeed, both experimental and TD-DFT predicted spectra show isoenergetic absorptions.

In their analysis of Pt(II) complexes with *bis*(2-pyridylimino)isoindole (BPI) and benzannulated ligand analogs, Hanson *et al.* noted that the HOMO of a 1,3-butadiene fragment has appropriate symmetry to act as an effective electron-donating group to the LUMO of the isoindole of BPI, and that the destabilization is due largely to this effect on the LUMO, as opposed to a significant influence on the HOMO.[27] The orbital contributions to the frontier orbitals of the Pt complexes presented here similarly reveal that the LUMO/LUMO+1 (but not the HOMO) present lobes of the appropriate symmetry at the site of benzannulation to interact with the HOMO of a 1,3-butadiene moiety. While the LUMO+1 is slightly destabilized upon benzannulation, consistent with the fused 1,3-butadiene moiety acting as an effective electron donor, benzannulation has a more conventional impact on the LUMO, which drops in energy. Our ligand design therefore can be contrasted with the experimental paradigm previously put forward as a general explanation for blue-shifted emission in benzannulated ligands.[27] In this case, the nearly 40 nm blue shift in the emission maximum cannot be solely explained by the impact of site-specific benzannulation on ligand electronics.

Table 2. TD-DFT vertical excitation energies and HOMO, LUMO, and LUMO+1 energies for complexes **1-3**.

	Orbital Energies (eV)			λ_{calc} /nm	Assignment	Oscillator Strength	Coefficient	% Contribution
	HOMO	LUMO	LUMO+1					
1	-5.31	-1.97	-1.96	506.7	HOMO→LUMO+1	0.3263	0.70258	98.7
2	-5.31	-2.02	-1.93	504.7	HOMO→LUMO+1	0.3637	0.70136	98.4
3	-5.29	-2.05	-1.92	505.7	HOMO→LUMO+1	0.3884	0.70193	98.5

To investigate the origin of this curious blue shift, the complexes were optimized with triplet multiplicities to compare the energies of the lowest lying triplet states (T_1) with estimates of the first excited singlet states from TD-DFT (Table S14, Figure S15). Calculated single-point energies of the complexes at the optimized triplet geometry with singlet multiplicity ($T_1@S_0$; Figure S15) were used to computationally estimate emission energies. Consistent with experimentally observed phosphorescence, the T_1 state for **3** indeed lies higher in energy relative to its ground state (S_0; 1.88 eV) compared to the energies of the T_1 states calculated for **1** and **2**. In addition, the corresponding calculated emission energy $E(T_1) - E(T_1@S_0)$ is also higher for the largest π-system (1.63 eV for **3** vs 1.51 (**1**) and 1.49 (**2**)), again reproducing experiment.

Comparing the optimized geometries of the ground state (S_0) and first excited state (T_1) of **1**, **2** and **3** reveals structural changes that accompany emission (Figure 6; Tables S15-S16). The root-mean-squared deviations, calculated from overlaying the optimized S_0 and T_1 structures (**1**: 0.328 Å, **2**: 0.356; **3**: 0.295; Figure S16), are consistent with bigger structural differences for the smaller quinolinyl-containing systems (**1** and **2**) compared with **3**. In all three ground-state structures, the rigid tridentate ligand maintains a highly planar orientation. In their T_1 excited states, the two ligand arms twist to break this plane, which likely contributes strongly to the rates of non-radiative decay.[47] In particular, a strong torsional twist of up to ~ 13° is observed. For example, while similar torsions are observed for the optimized T_1 geometries for **2** (13.2°) and **3** (12.8°), the deviation from the planarity of the ligand in the triplet geometry compared with the

ground state is more pronounced for **2** (S_1 4.2, T_1 13.2; Δ = 9.0) than for **3** (S_1 7.6, T_1 12.8; Δ = 5.2).

With respect to the *N*-heterocyclic moieties themselves, the C_5N sub-unit in the quinolinyl moiety in **1** in the T_1 excited state is more significantly distorted compared with the benzannulated C_5N sub-unit in the phenanthridinyl moiety of the ligand in **3** (Figure S17). The largest change in the phenanthridinyl moiety is localized in the C=N sub-unit, consistent with localization of double-bond character in this position which maximizes the number of aromatic sextets in the fused three ring system.[48] This buffers the phenanthridinyl ring system from larger overall changes compared with quinoline. Comparing all three complexes, the C_5N rings of the calculated T_1 structures are all strongly distorted in one half of the tridentate ligand only: in **1** and **2**, this is the quinolinyl arm; in **3**, a phenanthridinyl. This is consistent with isoenergetic emission from **1** and **2**, as the emissive excited state in both involves the quinoline (rather than the phenanthridine).

This implies that the higher energy triplet state of **3** can also be attributed to inhibition of the electronically desirable distortion for **3** compared with **1** or **2**. A similar observation has been made for cyclometallated Pt complexes with extended π-systems[42] and for Cu emitters.[43] With respect to the cyclometallated Pt complexes, the extent of π-conjugation in aromatic *C^N* ligands was found to also *not* correspond with the observed trends in emission energies, and was rationalized in terms of structural distortions that occur upon cyclometalation matching distortions that stabilized the molecules' triplet states. The energy cost of geometry relaxation of the T_1 state to the S_0 state has been previously estimated by calculating the corresponding relaxation energy (λ_T).[49] For **3**, the λ_T (0.25 eV) is smaller than those determined for **1** and **2** (0.28, 0.27 eV respectively), though these values are close to being within error of each other. Nevertheless, the observed and measurable geometric changes are consistent with the phenanthridinyl *P^N* ligands enforcing an excited state geometry more similar to the ground state geometry in **3** than for the smaller quinolinyl-containing analogs **1** and **2** with a commensurately smaller resulting apparent Stokes shift.

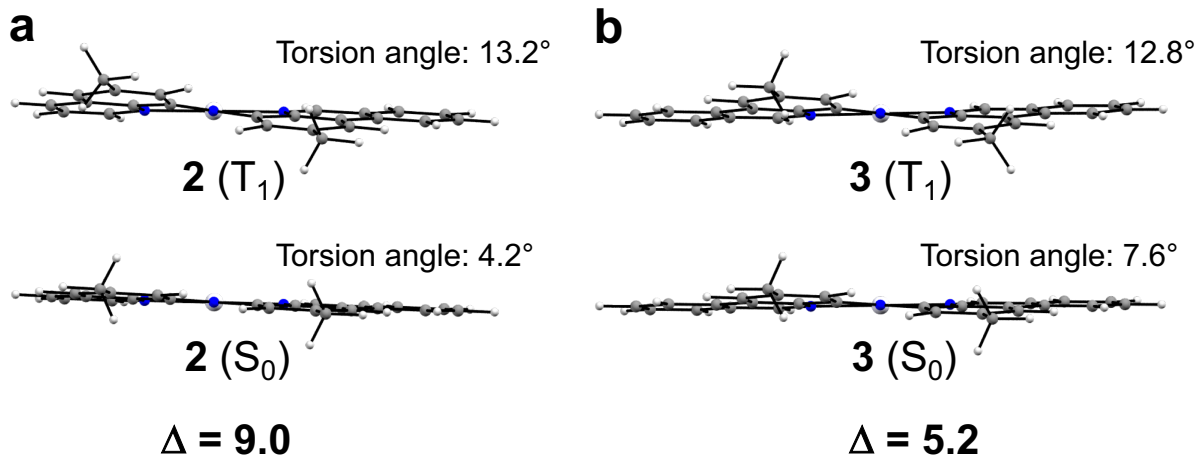

Figure 6. Comparison of torsion angles in DFT-optimized structures of S_0 and T_1 states of **2** and **3**.

CONCLUSION

The complexes discovered during this study are amongst the most red-shifted of phosphorescent Pt(II) complexes reported to date that emit from monomolecular excited states. While emission peaking around 700 nm in solution is well-established for bimolecular (aggregate or excimer) excited states of Pt(II) complexes,[50-51] complexes with sufficient conjugation to emit in this region from monomolecular states are rare and are largely limited to platinum porphyrins and phthalocyanins. Of particular interest also is the observation of the intense low-energy absorption band around 500 nm. For many applications, particularly those envisaged for use in biological media such as biosensing and imaging, intense absorption in the visible region is desirable.[3] The "brightness" of the phosphor – defined as the product of the emission quantum yield and the extinction coefficient at the excitation wavelength – is crucial. Similar criteria apply to the development of materials for photodynamic therapy (PDT) where low-energy excitation is sought, beyond the wavelength range where endogenous biological molecules absorb strongly.[52-53] In PDT, long-lived excited states that can sensitize the formation of singlet oxygen are desirable, and the efficient excited-state quenching by oxygen observed in this new series of complexes (Table 1) suggests that such a process is at work. The

availability of molecules with intense visible absorption in conjunction with efficient formation of triplet states having microsecond lifetimes is similarly desirable for upconversion through triplet-triplet annihilation (TTA-UC).[54]

In general, molecular-level control over emission properties is critical to designing useful light-emitting materials. Ligand benzannulation and the resultant extension of a molecule's π-system have long been successfully exploited to narrow HOMO-LUMO gaps and shift absorption/emission to the red. The work of Thompson and colleagues[27] demonstrated that a more nuanced consideration of the impact of benzannulation on frontier orbital energies can also predict 'counter-intuitive' shifts in absorption/emission energy that sometimes accompany π-extension. Here, we present a further exception, wherein combining quinolinyl and phenanthridinyl arms in ligand frameworks results in complexes where absorption and emission are not impacted in the same direction by benzannulation. The findings of this study will hopefully serve as an additional tool for materials designers.

Experimental Section

General Information

All air-sensitive manipulations were carried either in a N_2-filled glove box or using standard Schlenk techniques under Ar. $Pd_2(dba)_3$, (±)-2,2′-*bis*(diphenylphosphino)-1,1′-binaphthalene (*rac*-BINAP), and sodium *tert*-butoxide (NaO*t*Bu) were purchased (Sigma Aldrich) and used without further purification. 8-Bromo-6-methylquinoline,[33] 8-amino-6-methylquinoline,[55] $Pt(COD)Cl_2$,[56] 4-amino-2-methylphenanthridine, **L3** and **3**[35] were synthesized according to literature procedures. Organic solvents were dried and distilled using appropriate drying agents, and distilled water was degassed prior to use. 1- and 2D NMR spectra were recorded on Bruker Avance 300 MHz or Bruker Avance – III 500 MHz spectrometers. ^1H and $^{13}C\{^1H\}$ NMR spectra (Figures S18-S23) were referenced to residual solvent peaks.[57] Elemental analyses were performed by Microanalytical Service Ltd., Delta, BC (Canada) and at the University of Manitoba using a Perkin Elmer 2400

Series II CHNS/O Elemental Analyzer. Thermogravimetric analyses (TGA) were recorded on a Perkin Elmer TGA 7 instrument under an argon atmosphere.

General Procedure for Proligand Synthesis (L1-L2):

A thick-walled, 100 mL Teflon-stoppered flask was charged with $Pd_2(dba)_3$, *rac*-BINAP and toluene (30 mL) in the amounts noted below. After stirring briefly, the appropriate quinoline or phenanthridine reagents were added, along with an additional 30 mL of toluene, followed by the alkoxide base. The sealed flask was then stirred vigorously for 72 h in an oil bath set to 150 °C. After cooling and removing the volatiles, the residue was taken up in CH_2Cl_2 (120 mL) with the resulting suspension filtered over Celite and dried.

^{Me,Quin}NN(H)N^{Quin,Me} (L1): The general procedure was followed using: $Pd_2(dba)_3$ (84.0 mg, 0.09 mmol), *rac*-BINAP (112.6 mg, 0.18 mmol); 8-bromo-6-methylquinoline (0.36 g, 2.27 mmol), 8-amino-6-methylquinoline (0.50 g, 2.26 mmol); and NaO*t*Bu (0.26 g, 2.71 mmol). Column chromatography gave a yellow solid (neutral alumina; 1:5 EtOAc/hexane; R_f = 0.5). Isolated yield = 0.67 g (98%). ^{1}H NMR ($CDCl_3$, 300 MHz, 22 °C): δ 10.55 (br s, 1H; N*H*), 8.88 (dd, 2H, J_{HH} = 4.2, 1.7 Hz; $C_{Ar}H$), 8.04 (dd, 2H, J_{HH} = 8.2, 1.7 Hz; $C_{Ar}H$), 7.74 (d, 2H, J_{HH} = 1.6 Hz; $C_{Ar}H$), 7.41 (dd, 2H, J_{HH} = 8.2, 4.2 Hz; $C_{Ar}H$), 7.11 (bs, 2H, $C_{Ar}H$), 2.58 ppm (s, 6H; CH_3). ^{13}C{^{1}H} NMR ($CDCl_3$, 75 MHz, 22 °C): δ 147.4 (C_{Ar}), 139.0 (C_{Ar}), 138.6 (C_{Ar}), 137.1 (C_{Ar}), 135.5 (C_{Ar}), 129.1 (C_{Ar}), 121.8 (C_{Ar}), 117.0 (C_{Ar}), 112.0 (C_{Ar}), 22.7 ppm (CH$_3$).

^{Me,Phen}NN(H)N^{Quin,Me} (L2): The general procedure was followed using: $Pd_2(dba)_3$ (0.174 g, 0.180 mmol), *rac*-BINAP (0.275 g, 0.440 mmol); 8-bromo-6-methylquinoline (0.700 g, 3.15 mmol), 4-amino-2-methylphenanthridine[35] (0.660 g, 3.15 mmol); and NaO*t*Bu (0.450 g, 4.73 mmol). Column chromatography gave a yellow solid (neutral alumina; 1:5 EtOAc/hexane; R_f = 0.3). Isolated yield = 1.01 g (92%). ^{1}H NMR ($CDCl_3$, 300 MHz, 22 °C): δ 10.60 (br s, 1H; N*H*), 9.27 (s, 1H; $C_{Ar}H$), 8.90 (d, 1H, J_{HH} = 4.1 Hz; $C_{Ar}H$), 8.60 (d, 1H, J_{HH} = 8.3 Hz; $C_{Ar}H$), 8.11-8.00 (overlapped m, 2H; $C_{Ar}H$), 7.88-7.81 (overlapped m, 3H; $C_{Ar}H$), 7.76 (s, 1H; $C_{Ar}H$), 7.69 (app t, 1H, J_{HH} = 7.4 Hz; $C_{Ar}H$), 7.40 (dd, 1H, J_{HH} = 8.2, 4.2 Hz; $C_{Ar}H$), 7.10 (s, 1H; $C_{Ar}H$), 2.67 ppm (s, 3H; $C_{Phen}H_3$), 2.58 (s, 3H; $C_{Quin}H_3$). ^{13}C{^{1}H} NMR ($CDCl_3$, 75 MHz, 22 °C): δ 150.2 (C_{Ar}), 147.3 (C_{Ar}), 139.5

(C_{Ar}), 139.0 (C_{Ar}), 138.8 (C_{Ar}), 137.1 (C_{Ar}), 135.5 (C_{Ar}), 133.9 (C_{Ar}), 132.7 (C_{Ar}), 130.6 (C_{Ar}), 129.2 (C_{Ar}), 128.8 (C_{Ar}), 127.3 (C_{Ar}), 127.0 (C_{Ar}), 124.8 (C_{Ar}), 122.5 (C_{Ar}), 121.7 (C_{Ar}), 116.9 (C_{Ar}), 112.8 (C_{Ar}), 112.6 (C_{Ar}), 111.9 (C_{Ar}), 23.0 ($C_{Phen}H_3$), 22.7 ppm ($C_{Quin}H_3$).

General Procedure for Pt Complex Synthesis: In a thick-walled Teflon-stoppered flask, equimolar amounts of $Pt(COD)Cl_2$[56] and NaO*t*Bu were added to a solution of the appropriate ligand (**L1**, **L2** or **L3**) in 10 mL of CH_2Cl_2, and the mixture stirred vigorously at 70 °C for 18 h. The resulting red suspension was allowed to cool, and the volatiles were removed *in vacuo*. The residue was then was washed with acetonitrile (3 x 10 mL) and diethylether (3 x 10 mL).

^{Me,Quin}NNN^{Quin,Me}-PtCl (1): The general procedure was followed using: **L1** (0.15 g, 0.50 mmol), $Pt(COD)Cl_2$ (0.19 g, 0.51 mmol), and NaO*t*Bu (0.05 g, 0.52 mmol). Isolated yield = 0.217 g (82 %). ^{1}H NMR ($CDCl_3$, 300 MHz, 22 °C): δ 9.13 (dd, 2H, J_{HH} = 5.2, 1.4 Hz; $C_{Ar}H$), 8.17 (d, 2H, J_{HH} = 8.4 Hz; $C_{Ar}H$), 7.51 (s, 2H, $C_{Ar}H$), 7.36 (dd, 2H, $J_{H\text{-}H}$ = 8.3, 5.1 Hz; $C_{Ar}H$), 6.89 (s, 2H, $C_{Ar}H$), 2.59 ppm (s, 6H, CH_3). Anal. Calcd for $C_{20}H_{16}ClN_3Pt$: C, 45.42; H, 3.05. Found: C, 44.70; H, 3.27.

Synthesis of ^{Me,Phen}NNN^{Quin,Me}-PtCl (2): The general procedure was followed using: **L2** (0.20 g, 0.58 mmol), $Pt(COD)Cl_2$ (0.22 g, 0.59 mmol), and NaO*t*Bu (0.060 g, 0.60 mmol). Isolated yield = 0.266 g (79 %). ^{1}H NMR ($CDCl_3$, 300 MHz, 22 °C): δ 9.50 (s, 1H, $C_{Ar}H$), 9.10 (d, 1H, J_{HH} = 4.8 Hz; $C_{Ar}H$), 8.43 (d, 1H, J_{HH} = 8.4 Hz; $C_{Ar}H$), 8.11 (d, 1H, J_{HH} = 8.3 Hz; $C_{Ar}H$), 8.02 (d, 1H, J_{HH} = 7.9 Hz; $C_{Ar}H$), 7.87 (app t, 1H, J_{HH} = 7.7 Hz; $C_{Ar}H$), 7.67 (app t, 1H, J_{HH} = 7.5 Hz; $C_{Ar}H$), 7.54 (s, 1H, $C_{Ar}H$), 7.49 (s, 1H, $C_{Ar}H$), 7.45 (s, 1H, $C_{Ar}H$), 7.32 (dd, 1H, J_{HH} = 8.3, 5.0 Hz; $C_{Ar}H$), 6.78 (s, 1H, $C_{Ar}H$), 2.62 (s, 3H, CH_3), 2.55 ppm (s, 3H, CH_3). Anal. Calcd for $C_{24}H_{18}ClN_3Pt$: C, 49.79; H, 3.13. Found: C, 49.49; H, 3.20.

X-Ray Crystallography

X-ray crystal structure data was using collected from a multi-faceted crystals of suitable size and quality selected from a representative sample of crystals of the same habit using an optical microscope. The crystal was mounted on MiTiGen loops with data collection

carried out in a cold stream of nitrogen (150 K; Bruker D8 QUEST ECO; Mo K_α radiation). All diffractometer manipulations were carried out using Bruker APEX3 software.[58] Structure solution and refinement was carried out using XS and XL software, embedded within the Bruker SHELXTL suite.[59] The absence of additional symmetry was confirmed using ADDSYM incorporated in the PLATON program.[60] CCDC No. 1947217 contains the supplementary crystallographic data for this paper. The data can be obtained free of charge from The Cambridge Crystallographic Data Centre via www.ccdc.cam.ac.uk/structures.

Crystal structure data for **1**: X-ray quality crystals were grown following diffusion of diethylether vapor into a $CHCl_3$ of the compound at room temperature. Crystal structure parameters: $C_{20}H_{16}Cl_1N_3Pt_1$ 528.90 g/mol, monoclinic, space group $P2_1/n$; a = 9.8984(3) Å, b = 7.6056(3) Å, c = 21.7673(7) Å, α = 90°, β = 98.1820(10)°, γ = 90°, V = 1622.03(10) $Å^3$; Z = 4, ρ_{calcd} = 2.166 g cm^{-3}; crystal dimensions 0.110 x 0.080 x 0.020 mm^3; θ_{max} = 27.525°; 36146 reflections, 3726 independent (R_{int} = 0.0672), direct methods; absorption coeff (μ = 8.823 mm^{-1}), absorption correction semi-empirical from equivalents (SADABS); refinement (against F_o^2) with SHELXTL V6.1, 228 parameters, 0 restraints, R_1 = 0.0287 ($I > 2\sigma$) and wR_2 = 0.0617 (all data), Goof = 1.066, residual electron density 1.285/−0.880 e $Å^{-3}$.

Thermal Gravimetric Analysis

Thermal gravimetric analysis was performed on 2-3 mg of each complex. The temperature was started initially at 50 °C and ramped to 500 °C for the corresponding complexes at the following rates: **1**: 1 °C/min; **2**: 50 °- 200 °C at 5 °C/min; 200 °C – 500 °C at 2 °/min; **3**: 50 °- 200 °C at 5 °C/min; 200 °C – 500 °C at 2 °/min.

Optical Spectroscopy Measurements

The absorption spectra of the complexes were measured in solution in CH_2Cl_2 in 1 cm quartz cuvettes using a Biotek Instruments XS UV-visible spectrometer at room temperature. The emission spectra of the proligands at 295 and 77 K, and of their Pt(II)

complexes at 77 K, were recorded using a Jobin Yvon Fluoromax-2 spectrometer equipped with a red-sensitive Hamamatsu R928 photomuliplier tube. The emission spectra of the Pt(II) complexes at 295 K, which extend up to around 1000 nm, were recorded using a thermoelectrically cooled Synapse CCD detector, which offers better sensitivity in the red / NIR region compared to the R928 PMT. The samples for measurements at 295 K were contained within 1 cm pathlength quartz cuvettes modified for attachment to a vacuum line, and were degassed prior to measurement by a minimum of three freeze-pump-thaw cycles; final vapor pressure at 77 K was $< 10^{-2}$ mbar. Emission spectra at 77 K were recorded in 4 mm diameter tubes held within a liquid-nitrogen-cooled quartz dewar. Luminescence lifetimes were measured by time-correlated single-photon counting (TCSPC) following excitation using a pulsed laser diode at 405 nm; the emitted light was detected at right angles to the excitation beam, using an R928 PMT thermoelectrically cooled to –20°C.

Calculations

DFT calculations were carried out using Gaussian09[61] with M062x/LANL2DZ[62-63] with an IEFPCM[64] solvent model with DCM. TD-DFT calculations were performed with M06/LANL2DZ[62-63]on the M062x/LANL2DZ optimized structures. Molecular orbital analyses were carried out with Hirshfeld partition method[46] available in Multiwfn software.[65] and visualized using VESTA,[66] while TD-DFT results were analyzed using Origin 2017 software package.

To calculate ground-state, excited-state and reorganization energies,[49] the following protocol was followed: (1) The S_0 geometry was optimized by restricted DFT (charge = 0, multiplicity = 1) using the crystal structure coordinates as starting input. The T_1 geometry was optimized with unrestricted DFT (charge = 0, multiplicity = 3) using the optimized S_0 geometry as starting input. Frequency calculations were then subsequently carried out to confirm that these structures are at a minimum and to derive free energies. (2) To determine the relative atomic contributions to the frontier MOs, population analyses were carried out on the optimized structures of S_0 states. The electronic energies, $E(S_0)$ and $E(T_1)$, obtained from the single point calculations of S_0 and T_1 in their

respective minimum were used to estimate the adiabatic energy (E^{adia}), where, $E^{adia} = E(T_1) - E(S_0)$. (3) TD-DFT was then carried out on the following: (a) $S_n \leftarrow S_0$ singlet-singlet transitions (first 50 transitions) with the restricted formalism with charge = 0 and multiplicity = 1; (b) $T_n \leftarrow (T_1@S_0)$ singlet-triplet transitions (first 50 transitions) with the unrestricted formalism, but keeping the same charge and multiplicity as in (a). These gave $E^{vert\text{-}abs}$ and $E^{vert\text{-}phos}$ as shown in Figure S15. The reorganization energy (λ_T) after the emission of light was then calculated as $\lambda_T = E^{adia} - E^{vert\text{-}phos}$. As shown in Figure S15, "$T_1@S_0$" denotes a single point calculation on the singlet potential energy surface (*i.e.*, with singlet multiplicity) with a geometry matching that of optimized T_1 structure.

ASSOCIATED CONTENT

Supporting Information. Multi-nuclear NMR spectra of all new compounds; additional UV-Vis absorption and emission spectra; details of computational methods; crystallographic information file containing X-ray data with embedded structure factors and .res file. CCDC 1947217 contains the supplementary crystallographic data for this paper. The data can be obtained free of charge from The Cambridge Crystallographic Data Centre via www.ccdc.cam.ac.uk/structures.

The following files are available free of charge:
Supporting Information File (PDF)
Crystallographic Information File for **1** (CIF)

AUTHOR INFORMATION

Corresponding Authors

ORCID

Pavan Mandapati: 0000-0002-3686-4850
Jason D. Braun: 0000-0002-5850-8048
Rebecca L. Davis: 0000-0002-0679-6025

David E. Herbert: 0000-0001-8190-2468

J. A. Gareth Williams: 0000-0002-4688-3000

Author Contributions

The manuscript was written through contributions of all authors. All authors have given approval to the final version of the manuscript.

ACKNOWLEDGMENTS

The following sources of funding are gratefully acknowledged: Natural Sciences Engineering Research Council of Canada for a Discovery Grant to DEH (RGPIN-2014-03733); the Canadian Foundation for Innovation and Research Manitoba for an award in support of an X-ray diffractometer (CFI #32146); the University of Manitoba for start-up funding (DEH), a UMGF PhD Fellowship (JDB) and GETS support (PM, JDB, CK). The Association of Commonwealth Universities (ACU) is thanked for a University of Manitoba Titular Fellowship (2016–17) to JAGW. Johan van Lierop and Rachel Nickel are gratefully acknowledged for use of, and assistance with, a TGA, as are Viktor N. Nemykin and Tanner Blesener for helpful discussions.

REFERENCES

1. Zhao, Q.; Li, F.; Huang, C. Phosphorescent Chemosensors Based on Heavy-Metal Complexes. *Chem. Soc. Rev.* **2010,** *39*, 3007-3030.

2. Wong, K. M.-C.; Yam, V. W.-W. Luminescence Platinum(II) Terpyridyl Complexes - From Fundamental Studies to Sensory Functions. *Coord. Chem. Rev.* **2007,** *251*, 2477-2488.

3. Baggaley, E.; Weinstein, J. A.; Williams, J. A. G. Lighting the Way to See Inside the Live Cell With Luminescent Transition Metal Complexes. *Coord. Chem. Rev.* **2012,** *256*, 1762-1785.

4. Mauro, M.; Aliprandi, A.; Septiadi, D.; Kehr, N. S.; De Cola, L. When Self-Assembly Meets Biology: Luminescent Platinum Complexes for Imaging Applications. *Chem. Soc. Rev.* **2014,** *43*, 4144-4166.

5. Chen, Y.; Guan, R.; Zhang, C.; Huang, J.; Ji, L.; Chao, H. Two-Photon Luminescent Metal Complexes for Bioimaging and Cancer Phototherapy. *Coord. Chem. Rev.* **2016,** *310*, 16-40.

6. *Highly Efficient OLEDs with Phosphorescent Materials*. Ed. Yersin, H.; Wiley-VCH: Weinheim, Germany, 2007.

7. Cebrian, C.; Mauro, M. Recent Advances in Phosphorescent Platinum Complexes for Organic Light-Emitting Diodes. *Beilstein J. Org. Chem.* **2018,** *14*, 1459-1481.

8. Kalinowski, J.; Fattori, V.; Cocchi, M.; Williams, J. A. G. Light-Emitting Devices Based on Organometallic Platinum Complexes as Emitters. *Coord. Chem. Rev.* **2011,** *255*, 2401-2425.

9. Wong, W.-Y.; Ho, C.-L. Heavy Metal Organometallic Electrophosphors Derived From Multi-Component Chromophores. *Coord. Chem. Rev.* **2009,** *253*, 1709-1758.

10. Chou, P.-T.; Chi, Y.; Chung, M.-W.; Lin, C.-C. Harvesting Luminescence Via Harnessing the Photophysical Properties of Transition Metal Complexes. *Coord. Chem. Rev.* **2011,** *255*, 2653-2665.

11. Li, K.; Ming Tong, G. S.; Wan, Q.; Cheng, G.; Tong, W.-Y.; Ang, W.-H.; Kwong, W.-L.; Che, C.-M. Highly Phosphorescent Platinum(II) Emitters: Photophysics, Materials and Biological Applications. *Chem. Sci.* **2016,** *7*, 1653-1673.

12. Williams, J. A. G. Photochemistry and Photophysics of Coordination Compounds: Platinum. *Top. Curr. Chem.* **2007,** *281*, 205-268.

13. Chou, P.-T.; Chi, Y. Phosphorescent Dyes for Organic Light-Emitting Diodes. *Chem. Eur. J.* **2007,** *13*, 380-395.

14. Zhou, G.; Wong, W.-Y.; Yang, X. New Design Tactics in OLEDs Using Functionalized 2-Phenylpyridine-Type Cyclometalates of Iridium(III) and Platinum(II). *Chem. Asian J.* **2011,** *6*, 1706-1727.

15. Williams, J. A. G. The Coordination Chemistry of Dipyridylbenzene: N-Deficient Terpyridine or Panacea for Brightly Luminescent Metal Complexes? *Chem. Soc. Rev.* **2009,** *38*, 1783-1801.

16. Murphy, L.; Williams, J. A. G. Luminescent Platinum Compounds: from Molecules to OLEDs. *Top. Organomet. Chem.* **2010,** *28*, 75-111.

17. Freeman, G. R.; Williams, J. A. G. Metal Complexes of pincer Ligands: Excited States, Photochemistry, and Luminescence. *Top. Organomet. Chem.* **2013,** *40*, 89-130.

18. Vezzu, D. A. K.; Ravindranathan, D.; Garner, A. W.; Bartolotti, L.; Smith, M. E.; Boyle, P. D.; Huo, S.-Q. Highly Luminescent Tridentate N-C*N Platinum(II) Complexes Featured in Fused Five-Six-Membered Metallacycle and Diminishing Concentration Quenching. *Inorg. Chem.* **2011,** *50*, 8261-8273.

19. Kong, F. K.-W.; Tang, M.-C.; Wong, Y.-C.; Ng, M.; Chan, M.-Y.; Yam, V. W.-W. Strategy for the Realization of Efficient Solution-Processable Phosphorescent Organic Light-Emitting Devices: Design and Synthesis of Bipolar Alkynylplatinum(II) Complexes. *J. Am. Chem. Soc.* **2017,** *139*, 6351-6362.

20. Chow, P.-K.; Cheng, G.; Tong, G. S. M.; To, W.-P.; Kwong, W.-L.; Low, K.-H.; Kwok, C.-C.; Ma, C.; Che, C.-M. Luminescent Pincer Platinum(II) Complexes with Emission Quantum Yields up to Almost Unity: Photophysics, Photoreductive C-C Bond Formation, and Materials Applications. *Angew. Chem., Int. Ed.* **2015,** *54*, 2084-2089.

21. Rausch, A. F.; Murphy, L.; Williams, J. A. G.; Yersin, H. Probing the Excited State Properties of the Highly Phosphorescent Pt(dpyb)Cl Compound by High-Resolution Optical Spectroscopy. *Inorg. Chem.* **2009,** *48*, 11407-11414.

22. Rausch, A. F.; Murphy, L.; Williams, J. A. G.; Yersin, H. Improving the Performance of Pt(II) Complexes for Blue Light Emission by Enhancing the Molecular Rigidity. *Inorg. Chem.* **2012,** *51*, 312-319.

23. Zhao, D.; Tang, X.; Liu, X.-Y.; Fan, J.; Liao, L.-S. Highly Luminescent Platinum(II) Complexes Based on Pyrazolo[1,5-f]phenanthridine-Containing Ligands. *Org. Electron.* **2017,** *50*, 473-479.

24. Wen, H.-M.; Wu, Y.-H.; Fan, Y.; Zhang, L.-Y.; Chen, C.-N.; Chen, Z.-N. Spectroscopic and Luminescence Studies on Square-Planar Platinum(II) Complexes with Anionic Tridentate 3-Bis(2-pyridylimino)isoindoline Derivatives. *Inorg. Chem.* **2010,** *49*, 2210-2221.

25. Wen, H.-M.; Wu, Y.-H.; Xu, L.-J.; Zhang, L.-Y.; Chen, C.-N.; Chen, Z.-N. Luminescent Square-Planar Platinum(II) Complexes With Tridentate 3-Bis(2-pyridylimino)isoindoline and Monodentate *N*-Heterocyclic Ligands. *Dalton Trans.* **2011,** *40*, 6929-6938.

26. Wen, H.-M.; Wang, J.-Y.; Li, B.; Zhang, L.-Y.; Chen, C.-N.; Chen, Z.-N. Phosphorescent Square-Planar Platinum-(II) Complexes of 1,3-Bis(2-pyridylimino)-isoindoline with a Monodentate Strong-Field Ligand. *Eur. J. Inorg. Chem.* **2013,** *2013*, 4789-4798.

27. Hanson, K.; Roskop, L.; Djurovich, P. I.; Zahariev, F.; Gordon, M. S.; Thompson, M. E. A Paradigm for Blue- or Red-Shifted Absorption of Small Molecules Depending on the Site of π-Extension. *J. Am. Chem. Soc.* **2010,** *132*, 16247-16255.

28. Peters, J. C.; Harkins, S. B.; Brown, S. D.; Day, M. W. Pincer-like Amido Complexes of Platinum, Palladium, and Nickel. *Inorg. Chem.* **2001,** *40*, 5083-5091.

29. Harkins, S. B.; Peters, J. C. Base-Promoted Benzene C-H Activation Chemistry at an Amido Pincer Complex of Platinum(II). *Organometallics* **2002,** *21*, 1753-1755.

30. Maiti, D.; Paul, H.; Chanda, N.; Chakraborty, S.; Mondal, B.; Puranik, V. G.; Lahiri, G. K. Synthesis, Structure,Spectral and Electron-Transfer Properties of Octahedral-$[Co^{III}(L)_2]^+$/$[Zn^{II}(L)_2]$ and Square Planar-$[Cu^{II}(L)\{OC(=O)CH_3\}]$ Complexes Incorporating Anionic Form of Tridentate *Bis*(8-quinolinyl)amine $[N_1C_9H_6\text{-}N_2\text{-}C_9H_6N_3, L^-]$ Ligand. *Polyhedron* **2004,** *23*, 831-840.

31. Betley, T. A.; Qian, B. A.; Peters, J. C. Group VIII Coordination Chemistry of a Pincer-Type Bis(8-quinolinyl)amido Ligand. *Inorg. Chem.* **2008,** *47*, 11570-11582.

32. Hofmann, A.; Dahlenburg, L.; van Eldik, R. Cyclometalated Analogues of Platinum Terpyridine Complexes: Kinetic Study of the Strong σ-Donor Cis and Trans

Effects of Carbon in the Presence of a π-Acceptor Ligand Backbone. *Inorg. Chem.* **2003,** *42*, 6528-6538.

33. Lee, C.-I.; Zhou, J.; Ozerov, O. V. Catalytic Dehydrogenative Borylation of Terminal Alkynes by a SiNN Pincer Complex of Iridium. *J. Am. Chem. Soc.* **2013,** *135*, 3560-3566.

34. Mondal, R.; Giesbrecht, P. K.; Herbert, D. E. Nickel(II), Copper(I) and Zinc(II) Complexes Supported by a (4-Diphenylphosphino)phenanthridine Ligand. *Polyhedron* **2016,** *108*, 156-162.

35. Mandapati, P.; Giesbrecht, P. K.; Davis, R. L.; Herbert, D. E. Phenanthridine-Containing Pincer-like Amido Complexes of Nickel, Palladium, and Platinum. *Inorg. Chem.* **2017,** *56*, 3674-3685.

36. Zander, M. The Significance of Donor-Acceptor Interactions in the External Heavy Atom Effect of Silver Nitrate on the Luminescence Behavior of Aza-Aromatic Systems and Carbazoles. *Z. Naturforsch., A* **1978,** *33A*, 998-1000.

37. Ho, C.-L.; Li, H.; Wong, W.-Y. Red to Near-Infrared Organometallic Phosphorescent Dyes for OLED Applications. *J. Organomet. Chem.* **2014,** *751*, 261-285.

38. Tan, G.; Chen, S.; Siu, C.-H.; Langlois, A.; Qiu, Y.; Fan, H.; Ho, C.-L.; Harvey, P. D.; Lo, Y. H.; Liu, L.; Wong, W.-Y. Platinum(II) Cyclometallates Featuring Broad Emission Bands and Their Applications in Color-Tunable OLEDs and High Color-Rendering WOLEDs. *J. Mater. Chem. C* **2016,** *4*, 6016-6026.

39. Tuong Ly, K.; Chen-Cheng, R.-W.; Lin, H.-W.; Shiau, Y.-J.; Liu, S.-H.; Chou, P.-T.; Tsao, C.-S.; Huang, Y.-C.; Chi, Y. Near-Infrared Organic Light-Emitting Diodes With Very High External Quantum Efficiency and Radiance. *Nat. Photon.* **2017,** *11*, 63-68.

40. Zhang, Y.; Luo, Q.; Zheng, W.; Wang, Z.; Lin, Y.; Zhang, E.; Lu, S.; Xiang, J.; Zhao, Y.; Wang, F. Luminescent Cyclometallated Platinum(II) Complexes: Highly Promising EGFR/DNA Probes and Dual-targeting Anticancer Agents. *Inorg. Chem. Front.* **2018,** *5*, 413-424.

41. Paul-Roth, C. O.; Drouet, S.; Merhi, A.; Williams, J. A. G.; Gildea, L. F.; Pearson, C.; Petty, M. C. Synthesis of Platinum Complexes of Fluorenyl-Substituted Porphyrins Used as Phosphorescent Dyes for Solution-Processed Organic Light-Emitting Devices. *Tetrahedron* **2013,** *69*, 9625-9632.

42. Bossi, A.; Rausch, A. F.; Leitl, M. J.; Czerwieniec, R.; Whited, M. T.; Djurovich, P. I.; Yersin, H.; Thompson, M. E. Photophysical Properties of Cyclometalated Pt(II) Complexes: Counterintuitive Blue Shift in Emission with an Expanded Ligand π System. *Inorg. Chem.* **2013,** *52*, 12403-12415.

43. Mondal, R.; Lozada, I. B.; Davis, R. L.; Williams, J. A. G.; Herbert, D. E. Site-Selective Benzannulation of N-Heterocycles in Bidentate Ligands Leads to Blue-Shifted Emission from $[(P\text{^}N)Cu]_2(\mu\text{-}X)_2$ Dimers. *Inorg. Chem.* **2018,** *57*, 4966-4978.

44. Shafikov, M. Z.; Daniels, R.; Pander, P.; Dias, F. B.; Williams, J. A. G.; Kozhevnikov, V. N. Dinuclear Design of a Pt(II) Complex Affording Highly Efficient

Red Emission: Photophysical Properties and Application in Solution-Processible OLEDs. *ACS Appl. Mater. Interfaces* **2019,** *11*, 8182-8193.

45. Englman, R.; Jortner, J. Energy Gap Law for Radiationless Transitions in Large Molecules. *Mol. Phys.* **1970,** *18*, 145-64.

46. Hirshfeld, F. L. Bonded-Atom Fragments for Describing Molecular Charge Densities. *Theor. Chim. Acta* **1977,** *44*, 129-38.

47. Tong, G. S. M.; Che, C.-M. Emissive or Nonemissive? A Theoretical Analysis of the Phosphorescence Efficiencies of Cyclometalated Platinum(II) Complexes. *Chem.-Eur. J.* **2009,** *15*, 7225-7237.

48. Maksić, Z. B.; Barić, D.; Müller, T. Clar's Sextet Rule Is a Consequence of the σ-Electron Framework. *J. Phys. Chem. A* **2006,** *110*, 10135-10147.

49. Uoyama, H.; Goushi, K.; Shizu, K.; Nomura, H.; Adachi, C. Highly Efficient Organic Light-Emitting Diodes From Delayed Fluorescence. *Nature* **2012,** *492*, 234-238.

50. Lai, S.-W.; Chan, M. C.-W.; Cheung, T.-C.; Peng, S.-M.; Che, C.-M. Probing d8-d8 Interactions in Luminescent Mono- and Binuclear Cyclometalated Platinum(II) Complexes of 6-Phenyl-2,2'-bipyridines. *Inorg. Chem.* **1999,** *38*, 4046-4055.

51. Cocchi, M.; Kalinowski, J.; Virgili, D.; Williams, J. A. G. Excimer-Based Red/Near-Infrared Organic Light-Emitting Diodes With Very High Quantum Efficiency. *Appl. Phys. Lett.* **2008,** *92*, 113302/1-113302/3.

52. McKenzie, L. K.; Sazanovich, I. V.; Baggaley, E.; Bonneau, M.; Guerchais, V.; Williams, J. A. G.; Weinstein, J. A.; Bryant, H. E. Metal Complexes for Two-Photon Photodynamic Therapy: A Cyclometallated Iridium Complex Induces Two-Photon Photosensitization of Cancer Cells under Near-IR Light. *Chem. Eur. J.* **2017,** *23*, 234-238.

53. Colombo, A.; Fontani, M.; Dragonetti, C.; Roberto, D.; Williams, J. A. G.; Scotto di Perrotolo, R.; Casagrande, F.; Barozzi, S.; Polo, S. A Highly Luminescent Tetrahydrocurcumin Ir(III) Complex with Remarkable Photoactivated Anticancer Activity. *Chem. Eur. J.* **2019,** *25*, 7948-7952.

54. Wu, W.; Zhao, J.; Guo, H.; Sun, J.; Ji, S.; Wang, Z. Long-Lived Room-Remperature Near-IR Phosphorescence of BODIPY in a Visible-Light-Harvesting N(caret)C(caret)N Pt^{II}-acetylide Complex With a Directly Metalated BODIPY Chromophore. *Chem. Eur. J.* **2012,** *18*, 1961-1968, S1961/1-S1961/25.

55. Medina Padilla, M.; Castro Morera, A.; Sanchez-Quesada, J.; Garcia Palomero, E.; Alonso Cascon, M.; Herrero Santos, S.; Vela Ruiz, M.; Usan Egea, P.; Rodriguez Villanueva, A. L. Triple Substituted Phenanthroline Derivatives for the Treatment of Neurodegenerative or Haematological Diseases or Conditions, or Cancer. *US20110306631A1*, 2011.

56. Clark, H. C.; Manzer, L. E. Reactions of (π-1,5-Cyclooctadiene)organoplatinum(II) Compounds and the Synthesis of Perfluoroalkylplatinum Complexes. *J. Organomet. Chem.* **1973,** *59*, 411-28.

57. Fulmer, G. R.; Miller, A. J. M.; Sherden, N. H.; Gottlieb, H. E.; Nudelman, A.; Stoltz, B. M.; Bercaw, J. E.; Goldberg, K. I. NMR Chemical Shifts of Trace Impurities: Common Laboratory Solvents, Organics, and Gases in Deuterated Solvents Relevant to the Organometallic Chemist. *Organometallics* **2010,** *29*, 2176-2179.

58. Bruker-AXS *APEX3 v2016.1-0*, Madison, Wisconsin, USA, 2016.

59. Sheldrick, G. M. A Short History of SHELX. *Acta Cryst.* **2008,** *A64*, 112-122.

60. Spek, A. L. Structure Validation in Chemical Crystallography. *Acta Cryst.* **2009,** *D65*, 148-155.

61. Frisch, M. J.; Trucks, G. W.; Schlegel, H. B.; Scuseria, G. E.; Robb, M. A.; Cheeseman, J. R.; Scalmani, G.; Barone, V.; Mennucci, B.; Petersson, G. A.; Nakatsuji, H.; Caricato, M.; Li, X.; Hratchian, H. P.; Izmaylov, A. F.; Bloino, J.; Zheng, G.; Sonnenberg, J. L.; Hada, M.; Ehara, M.; Toyota, K.; Fukuda, R.; Hasegawa, J.; Ishida, M.; Nakajima, T.; Honda, Y.; Kitao, O.; Nakai, H.; Vreven, T.; Montgomery, J. A.; Peralta, J. E.; Ogliaro, F.; Bearpark, M.; Heyd, J. J.; Brothers, E.; Kudin, K. N.; Staroverov, V. N.; Kobayashi, R.; Normand, J.; Raghavachari, K.; Rendell, A.; Burant, J. C.; Iyengar, S. S.; Tomasi, J.; Cossi, M.; Rega, N.; Millam, J. M.; Klene, M.; Knox, J. E.; Cross, J. B.; Bakken, V.; Adamo, C.; Jaramillo, J.; Gomperts, R.; Stratmann, R. E.; Yazyev, O.; Austin, A. J.; Cammi, R.; Pomelli, C.; Ochterski, J. W.; Martin, R. L.; Morokuma, K.; Zakrzewski, V. G.; Voth, G. A.; Salvador, P.; Dannenberg, J. J.; Dapprich, S.; Daniels, A. D.; Farkas; Foresman, J. B.; Ortiz, J. V.; Cioslowski, J.; Fox, D. J., Gaussian 09, Revision B.01. In *Gaussian 09, Revision B.01, Gaussian, Inc., Wallingford CT*, Wallingford CT, 2009.

62. Zhao, Y.; Truhlar, D. G. The M06 Suite of Density Functionals for Main Group Thermochemistry, Thermochemical Kinetics, Noncovalent Interactions, Excited States, and Transition Elements: Two New Functionals and Systematic Testing of Four M06-Class Functionals and 12 Other Functionals. *Theor. Chem. Acc.* **2008,** *120*, 215-241.

63. Dunning, T. H., Jr.; Hay, P. J., In *Modern Theoretical Chemistry*, Schaefer III, H. F., Ed. Plenum, New York, 1977; Vol. 3, pp 1-28.

64. Tomasi, J.; Mennucci, B.; Cammi, R. Quantum Mechanical Continuum Solvation Models. *Chem. Rev.* **2005,** *105*, 2999-3094.

65. Lu, T.; Chen, F. Multiwfn: A Multifunctional Wavefunction Analyzer. *J. Comput. Chem.* **2012,** *33*, 580-592.

66. Momma, K.; Izumi, F. VESTA 3 for Three-Dimensional Visualization of Crystal, Volumetric and Morphology Data. *J. Appl. Cryst.* **2011,** *44*, 1272-1276.